Title	Coupled-channel approach to strangeness S = -2 baryon-bayron interactions in lattice QCD
Author(s)	Sasaki, Kenji; Aoki, Sinya; Doi, Takumi; Hatsuda, Tetsuo; Ikeda, Yoichi; Inoue, Takashi; Ishii, Noriyoshi; Murano, Keiko
Citation	Progress of Theoretical and Experimental Physics (2015), 2015(11)
Issue Date	2015-11
URL	http://hdl.handle.net/2433/216695
Right	© The Author(s) 2015. Published by Oxford University Press on behalf of the Physical Society of Japan.; This is an Open Access article distributed under the terms of the Creative Commons Attribution License (http://creativecommons.org/licenses/by/4.0/), which permits unrestricted reuse, distribution, and reproduction in any medium, provided the original work is properly cited. Funded by SCOAP3
Type	Journal Article
Textversion	publisher

PTEP

Prog. Theor. Exp. Phys. **2015**, 113B01 (18 pages)
DOI: 10.1093/ptep/ptv144

Coupled-channel approach to strangeness $S = -2$ baryon–bayron interactions in lattice QCD

Kenji Sasaki[1,*], Sinya Aoki[1,2], Takumi Doi[3], Tetsuo Hatsuda[3], Yoichi Ikeda[3], Takashi Inoue[4], Noriyoshi Ishii[5], and Keiko Murano[5]
(on behalf of the HAL QCD Collaboration)

[1]*Center for Computational Sciences, University of Tsukuba, Tsukuba 305-8577, Japan*
[2]*Yukawa Institute for Theoretical Physics, Kyoto University, Kyoto 606-8502, Japan*
[3]*Theoretical Research Division, Nishina Center, RIKEN, Wako 351-0198, Japan*
[4]*Nihon University, College of Bioresource Sciences, Fujisawa 252-0880, Japan*
[5]*Research Center for Nuclear Physics (RCNP), Osaka University, Ibaraki, Osaka 567-0047, Japan*
*E-mail: kenjis@het.ph.tsukuba.ac.jp

Received April 17, 2015; Revised September 1, 2015; Accepted September 1, 2015; Published November 11, 2015

Baryon–baryon interactions with strangeness $S = -2$ with flavor SU(3) breaking are calculated for the first time by using the HAL QCD method extended to the coupled-channel system in lattice QCD. The potential matrices are extracted from the Nambu–Bethe–Salpeter wave functions obtained by the $2 + 1$-flavor gauge configurations of the CP-PACS/JLQCD Collaborations with a physical volume of $(1.93\ \text{fm})^3$ and with $m_\pi/m_K = 0.96, 0.90, 0.86$. The spatial structure and the quark mass dependence of the potential matrix in the baryon basis and in the SU(3) basis are investigated.

Subject Index B38, B64, D32, D34

1. Introduction

Studying the baryon–baryon (BB) interactions in the strangeness $S = -2$ channel is an important step to understanding hypernuclei such as double-Λ hypernuclei and Ξ hypernuclei (see, e.g., Refs. [1–3]) as well as exotic hadrons such as the H-dibaryon [4,5]. Moreover, the hyperon superfluidity in the cores of neutron stars is intimately related to the hyperon–hyperon interaction in the $S = -2$ channel [6]. Due to the limited experimental data, however, the BB interactions in the $S = -2$ channel are far from being realistic even under the constraints from the approximate flavor SU(3) symmetry. In addition, there are nearby two-baryon states in the $S = -2$ channel (e.g., $\Lambda\Lambda$ and $N\Xi$), so that the coupled-channel treatment is essential for studying the $S = -2$ system.

Recently, the BB interactions in the flavor SU(3) limit have been studied systematically in full QCD simulations on the lattice by the HAL QCD method (reviewed in Ref. [7]) for several different masses of the pseudo-scalar meson $m_{\text{PS}} = 470$–$1170\ \text{MeV}$ (see Ref. [8] and references therein). In this case, all the two-baryon thresholds are degenerate and the classification of the BB interactions in the flavor basis is applicable. An extension of the HAL QCD method beyond the inelastic threshold, which is relevant for BB interactions with flavor SU(3) breaking, has also been proposed to treat coupled-channel systems [9,10]. The main purpose of this paper is to study BB interactions in the $S = -2$ channel with explicit SU(3) breaking on the basis of the coupled-channel HAL QCD method developed in our previous works [9,10].

Funded by SCOAP[3]

We note here that the hyperon–nucleon scattering length away from the SU(3) symmetric limit was first evaluated by quench QCD simulation in Ref. [11] and later by full QCD simulations in Refs. [12,13], where Lüscher's finite-volume method was utilized. On the other hand, the hyperon–nucleon potentials, which provide much more information than the scattering lengths, were derived through the equal-time Nambu–Bethe–Salpeter (NBS) wave functions with the HAL QCD method in Refs. [14–16]. The present study can be regarded as a coupled-channel generalization of our previous works below the inelastic threshold.

This paper is organized as follows. In Sect. 2, we review the coupled-channel approach to the *BB* interactions by the HAL QCD method in lattice QCD. In Sect. 3, we define the baryon operators and baryon states. In Sect. 4, the numerical setup on the lattice is summarized. In Sect. 5, we present our numerical results for the *BB* potentials. A summary and our conclusions are given in Sect. 6.

2. Coupled-channel *BB* potentials

In this section, we briefly review the coupled-channel HAL QCD method [9,10] applicable to the inelastic scattering in which $a_1 + a_2 \to b_1 + b_2$, where $(a_1, a_2) \neq (b_1, b_2)$.

2.1. Formalism

We first define the equal-time NBS wave functions with the total energy W_i as

$$\begin{aligned}\psi^a_{W_i}(\vec{r})e^{-W_i t} &= \frac{1}{\sqrt{Z_{a_1}}\sqrt{Z_{a_2}}}\sum_{\vec{x}}\langle 0|B_{a_1}(\vec{x}+\vec{r},t)B_{a_2}(\vec{x},t)|B=2,W_i\rangle,\\ \psi^b_{W_i}(\vec{r})e^{-W_i t} &= \frac{1}{\sqrt{Z_{b_1}}\sqrt{Z_{b_2}}}\sum_{\vec{x}}\langle 0|B_{b_1}(\vec{x}+\vec{r},t)B_{b_2}(\vec{x},t)|B=2,W_i\rangle,\end{aligned} \tag{1}$$

where $B_{c_j}(\vec{x},t)$ with $c = a, b$ and $j = 1, 2$ denotes a local composite operator for a baryon B_{c_j} with its wave-function renormalization factor $\sqrt{Z_{c_j}}$. The state $|B = 2, W_i\rangle$ stands for a QCD asymptotic in-state with baryon number 2 and energy W_i. In the present exploratory studies, we assume that $\sqrt{Z_{a1}}\sqrt{Z_{a2}} = \sqrt{Z_{b1}}\sqrt{Z_{b2}}$, which implies that the flavor SU(3) breaking in the wave-function renormalization factor is not sizable in the present setup. The validity of this assumption is left for future studies.

In the asymptotic region at long distance, these NBS wave functions satisfy free Schrödinger-type equations as

$$\left(\frac{(k^c_i)^2}{2\mu^c} + \frac{\nabla^2}{2\mu^c}\right)\psi^c_{W_i}(\vec{r}) = 0, \quad r \equiv |\vec{r}| \to \infty, \tag{2}$$

where the corresponding asymptotic momentum k^c_i in the center-of-mass (CM) frame is defined through the relation

$$W_i = \sqrt{m^2_{c_1} + (k^c_i)^2} + \sqrt{m^2_{c_2} + (k^c_i)^2}, \tag{3}$$

with m_{c_j} being the mass of the baryon B_{c_j}, and the reduced mass μ^c being given by $1/\mu^c = 1/m_{c_1} + 1/m_{c_2}$. On the other hand, in the interaction region at short distance, we have

$$K^c(\vec{r}, W_i) = \left(\frac{(k^c_i)^2}{2\mu^c} + \frac{\nabla^2}{2\mu^c}\right)\psi^c_{W_i}(\vec{r}) \neq 0, \tag{4}$$

from which we define the energy-independent non-local potential matrix as

$$K^c(\vec{r}, W_i) = \sum_{c'=a,b} \int d^3r'\, U^c{}_{c'}(\vec{r}, \vec{r}')\, \psi^{c'}_{W_i}(\vec{r}'). \tag{5}$$

This is an extension of the HAL QCD definition for the potential to the coupled-channel case [9]. To handle the non-locality of the potential, we introduce the derivative expansion as $U(\vec{r}, \vec{r}') = (V_{\rm LO}(\vec{r}) + V_{\rm NLO}(\vec{r}) + \cdots)\delta(\vec{r} - \vec{r}')$, where the N^{n}LO term is of $O(\vec{\nabla}^n)$. At low energies, a good convergence of the derivative expansion has been confirmed for the *NN* case [17].

2.2. *Extraction of potential matrix*

In the leading order of the derivative expansion of the non-local potential, Eqs. (4) and (5) can be written as a coupled-channel form of the Schrödinger equation for two independent channels a and b,

$$\begin{pmatrix} \left(E_i^a - H_0^a\right)\psi^a_{W_i}(\vec{r}) \\ \left(E_i^b - H_0^b\right)\psi^b_{W_i}(\vec{r}) \end{pmatrix} = \begin{pmatrix} V^a{}_a(\vec{r}) & V^a{}_b(\vec{r}) \\ V^b{}_a(\vec{r}) & V^b{}_b(\vec{r}) \end{pmatrix} \begin{pmatrix} \psi^a_{W_i}(\vec{r}) \\ \psi^b_{W_i}(\vec{r}) \end{pmatrix}, \tag{6}$$

where the kinetic energy and the free Hamiltonian for channels $c = a, b$ are given by $E_i^c = \frac{(k_i^c)^2}{2\mu^c}$ and $H_0{}^c = -\frac{\nabla^2}{2\mu^c}$, respectively.

Two pairs of NBS wave functions, $\left\{\psi^a_{W_i}, \psi^b_{W_i}\right\}_{i=1,2}$, are necessary to extract the local potential matrix from the above coupled-channel equation. In the infinite volume, we can have two states, $|a, W\rangle$ and $|b, W\rangle$, with a given energy W, which are connected to the asymptotic scattering states if W is larger than $m_{a_1} + m_{a_2}$ and $m_{b_1} + m_{b_2}$. This implies that two nearby eigenstates, $|B = 2, W_1\rangle$ and $|B = 2, W_2\rangle$ with $W_1 - W_2 = O(L^{-2})$, exist even for finite volume. Suppose that $W_1 < W_2$ are the two lowest energies of two baryons in the finite volume. By using the wall-source operators $\mathcal{I}_a(t) = \overline{\left(B_{a_2} B_{a_1}\right)}(t)$ and $\mathcal{I}_b(t) = \overline{\left(B_{b_2} B_{b_1}\right)}(t)$,[1] the states $|B = 2, W_1\rangle$ and $|B = 2, W_2\rangle$ are created as

$$\mathcal{I}_c(0)|0\rangle = C_{c1}|B = 2, W_1\rangle + C_{c2}|B = 2, W_2\rangle + \cdots, \tag{7}$$

where the coefficient matrix C_{cj} can be determined from the two-baryon correlation functions. We then define the optimized source operators as

$$\begin{pmatrix} \mathcal{I}_{W_1}(t) \\ \mathcal{I}_{W_2}(t) \end{pmatrix} = \begin{pmatrix} C_{a1} & C_{a2} \\ C_{b1} & C_{b1} \end{pmatrix}^{-1} \begin{pmatrix} \mathcal{I}_a(t) \\ \mathcal{I}_b(t) \end{pmatrix}, \tag{8}$$

so that the four-point (4-pt) function $F^c_{\mathcal{I}_{W_i}}(\vec{r}, t)$ at large t behaves as

$$F^c_{\mathcal{I}_{W_i}}(\vec{r}, t) \equiv \langle 0|B_{c_1}(\vec{x} + \vec{r}, t) B_{c_2}(\vec{x}, t) \mathcal{I}_{W_i}(0)|0\rangle \simeq \psi^c_{W_i}(\vec{r}) e^{-W_i t} + O\left(e^{-W_3 t}\right) \tag{9}$$

[1] A detailed definition of the wall-source operators will be given in Sect. 4.

for $i = 1, 2$ and $c = a, b$, where W_3 corresponds to the 3rd state satisfying $W_1 < W_2 < W_3 < W_{j\geq 4}$. By using these 4-pt functions, the coupled-channel potential matrix can be determined as

$$\begin{pmatrix} V^a{}_a(\vec{r}) & V^a{}_b(\vec{r}) \\ V^b{}_a(\vec{r}) & V^b{}_b(\vec{r}) \end{pmatrix} \simeq \begin{pmatrix} (E_1^a - H_0^a)F^a_{\mathcal{I}_{W_1}}(\vec{r},t) & (E_2^a - H_0^a)F^a_{\mathcal{I}_{W_2}}(\vec{r},t) \\ (E_1^b - H_0^b)F^b_{\mathcal{I}_{W_1}}(\vec{r},t) & (E_2^b - H_0^b)F^b_{\mathcal{I}_{W_2}}(\vec{r},t) \end{pmatrix} \times \begin{pmatrix} F^a_{\mathcal{I}_{W_1}}(\vec{r},t) & F^a_{\mathcal{I}_{W_2}}(\vec{r},t) \\ F^b_{\mathcal{I}_{W_1}}(\vec{r},t) & F^b_{\mathcal{I}_{W_2}}(\vec{r},t) \end{pmatrix}^{-1} \tag{10}$$

for sufficiently large t, where the states with $W(>W_1, W_2)$ can be neglected in the above 4-pt functions. As the volume increases, however, the spectrum becomes denser and the two low-lying states W_1 and W_2 cannot be isolated unless extremely large t is achieved. This is why we need an improved method in practice, as explained in the next subsection.

2.3. *Time-dependent method*

An improved method to extract the potentials without using ground-state saturation has been proposed in Ref. [18] in the case of the single channel. In this subsection, we extend this method to the coupled-channel case.

We first introduce the normalized 4-pt correlation function R, defined as

$$R^c_{\mathcal{I}_d}(\vec{r},t) \equiv \frac{F^c_{\mathcal{I}_d}(\vec{r},t)}{\exp[-(m_{c_1}+m_{c_2})t]} = \sum_j \psi^c_{W_j}(\vec{r}) e^{-\Delta W_j^c t} A_d^{W_j} + \cdots, \tag{11}$$

where $\Delta W_j^c = W_j - m_{c_1} - m_{c_2}$ and $A_d^{W_j} = \langle W_j | \mathcal{I}_d(0)|0\rangle$. The 4-pt function $F^c_{\mathcal{I}_d}(\vec{r},t)$ here is defined through the original wall-source operator $\mathcal{I}_d(0)$ instead of $\mathcal{I}_{W_i}(0)$. The ellipses in Eq. (11) denote inelastic contributions from channels other than a and b.

In the non-relativistic approximation valid at low energies, $\Delta W_j^c \simeq E_j^c$, we can replace the kinetic energy term in the equation with the time derivative as

$$-\frac{\partial}{\partial t} R^c{}_{\mathcal{I}_d}(\vec{r},t) \simeq \sum_j E_j^c \psi^c_{W_j}(\vec{r}) e^{-\Delta W_j t} A_d^{W_j}, \tag{12}$$

with which we obtain the Schrödinger-type equation

$$\left(-\frac{\partial}{\partial t} - H_0^c\right) R^c{}_{\mathcal{I}_d}(\vec{r},t) = \int d^3r' U^c{}_e(\vec{r},\vec{r}') \Delta^c{}_e R^e{}_{\mathcal{I}_d}(\vec{r}',t), \tag{13}$$

where $\Delta^c{}_e = \exp[-(m_{e_1}+m_{e_2})t]/\exp[-(m_{c_1}+m_{c_2})t]$. If we go beyond the non-relativistic approximation, higher-order time derivatives appear, which we will not consider in this paper. Expanding U in terms of derivatives again, the leading-order coupled-channel potentials can be obtained as

$$\begin{pmatrix} V^a{}_a(\vec{r}) & V^a{}_b(\vec{r})\Delta^a{}_b \\ V^b{}_a(\vec{r})\Delta^b{}_a & V^b{}_b(\vec{r}) \end{pmatrix} \simeq \begin{pmatrix} \left(-\frac{\partial}{\partial t} - H_0^a\right) R^a_{\mathcal{I}_a}(\vec{r},t) & \left(-\frac{\partial}{\partial t} - H_0^a\right) R^a_{\mathcal{I}_b}(\vec{r},t) \\ \left(-\frac{\partial}{\partial t} - H_0^b\right) R^b_{\mathcal{I}_a}(\vec{r},t) & \left(-\frac{\partial}{\partial t} - H_0^b\right) R^b_{\mathcal{I}_b}(\vec{r},t) \end{pmatrix} \times \begin{pmatrix} R^a_{\mathcal{I}_a}(\vec{r},t) & R^a_{\mathcal{I}_b}(\vec{r},t) \\ R^b_{\mathcal{I}_a}(\vec{r},t) & R^b_{\mathcal{I}_b}(\vec{r},t) \end{pmatrix}^{-1}. \tag{14}$$

Table 1. Summary of channels with $S = -2$.

	Channel	Baryon pairs	SU(3) multiplets
$I = 0$	${}^1S_0$	$\Lambda\Lambda$, $(N\Xi)_0$, $(\Sigma\Sigma)_0$	$1, 8_s, 27$
	${}^3S_1 - {}^3D_1$	$(N\Xi)_0$	8_a
$I = 1$	${}^1S_0$	$(N\Xi)_1$, $(\Lambda\Sigma)_1$	$8_s, 27$
	${}^3S_1 - {}^3D_1$	$(N\Xi)_1$, $\Lambda\Sigma$, $(\Sigma\Sigma)_1$	$8_a, 10, \overline{10}$
$I = 2$	${}^1S_0$	$(\Sigma\Sigma)_2$	27

Extension of this formula to three channels is straightforward. For Eq. (14) to work, two independent source operators $\mathcal{I}_a$ and $\mathcal{I}_b$ are needed, while no optimization is required. Note that isolation of each eigenstate is not necessary in this method [18]. The only constraint is to keep moderately large t so that other channels with larger threshold energies than a and b can be suppressed. In the following, we employ this improved method in our numerical calculations.

3. Strangeness $S = -2$ two-baryon system

We emply the following interpolating operator for octet baryons:

$$B_\alpha(\vec{x}) = \epsilon_{abc}\left(q_a^T(\vec{x})C\gamma_5 q_b(\vec{x})\right)q_{c\alpha}(\vec{x}) \tag{15}$$

with the Dirac index α, which represents the spin of the octet baryons. Denoting the quark flavors as $q = u, d, s$ for "up", "down", and "strange", respectively, the flavor structures of the baryons are given in terms of the isospin multiplets as

$$\begin{array}{llll} S=0 & I=1/2 & : & p=[ud]u\ , \qquad\qquad n=[ud]d \\ S=-1 & I=1 & : & \Sigma^+=-[us]u\ ,\ \Sigma^0=-([ds]u+[us]d)/\sqrt{2}\ ,\ \Sigma^-=-[ds]d \\ S=-1 & I=0 & : & \Lambda=([sd]u+[us]d-2[du]s)/\sqrt{6} \\ S=-2 & I=1/2 & : & \Xi^0=[su]s\ , \qquad\qquad \Xi^-=[sd]s \end{array} \tag{16}$$

Considering the Fermi–Dirac statistics of two baryons, the allowed combinations for the $S = -2$ system are given in Table 1, where the $I_z = 0$ components are given as

$$(\Sigma\Sigma)_I = \begin{cases} \sqrt{\frac{1}{3}}\left(\Sigma^+\Sigma^- + \Sigma^-\Sigma^+ - \Sigma^0\Sigma^0\right), & I=0 \\ \sqrt{\frac{1}{2}}\left(\Sigma^+\Sigma^- - \Sigma^-\Sigma^+\right), & I=1 \\ \sqrt{\frac{1}{6}}\left(\Sigma^+\Sigma^- + \Sigma^-\Sigma^+ + 2\Sigma^0\Sigma^0\right), & I=2 \end{cases} \tag{17}$$

$$(N\Xi)_I = \begin{cases} \sqrt{\frac{1}{2}}\left(p\Xi^- - n\Xi^0\right), & I=0 \\ \sqrt{\frac{1}{2}}\left(p\Xi^- + n\Xi^0\right), & I=1 \end{cases}. \tag{18}$$

4. Numerical simulations

We employ $2+1$-flavor full QCD gauge configurations from the Japan Lattice Data Grid (JLDG)/International Lattice Data Grid (ILDG) [19,20]. They are generated by the CP-PACS and JLQCD Collaborations [21] with the renormalization-group-improved gauge action and the non-perturbatively $O(a)$-improved Wilson quark action at $\beta = 6/g^2 = 1.83$ (corresponding lattice spacing in the physical unit, $a = 0.1209$ fm [22]) on an $L^3 \times T = 16^3 \times 32$ lattice (corresponding

Table 2. Lattice parameters and hadron masses in units of MeV are listed.

Lattice parameters					
β	κ_s	c_{SW}	lattice size	a [fm]	L [fm]
1.83	0.137 10	1.7610	$16^3 \times 32$	0.1209	1.93

	N_{conf}	κ_{ud}	m_π	m_K	m_N	m_Λ	m_Σ	m_Ξ
Set 1	700	0.137 60	875(1)	916(1)	1810(2)	1839(2)	1846(2)	1872(2)
Set 2	800	0.138 00	749(1)	828(1)	1619(2)	1675(2)	1689(2)	1737(2)
Set 3	800	0.138 25	660(1)	768(1)	1482(3)	1556(3)	1575(3)	1640(2)

lattice size in the physical unit, $(1.93\ \text{fm})^3 \times 3.87\ \text{fm}$). In our calculation, the hopping parameter for the s quark is kept as $\kappa_s = 0.137\,10$, while three gauge ensembles, $\kappa_{u,d} = 0.137\,60$ (Set 1), 0.138 00 (Set 2), and 0.138 25 (Set 3), are taken for the u, d quarks.

Wall-source operators that generate positive-parity two-baryon states with flavor structures h_1 and h_2 are given by

$$\mathcal{I}^h_{\alpha\beta} = \left[\epsilon_{abc}\left(\bar{Q}_a C\gamma_5 \bar{Q}_b^T\right)\bar{Q}_{c\alpha}\right]_{h_2}\left[\epsilon_{def}\left(\bar{Q}_d C\gamma_5 \bar{Q}_e^T\right)\bar{Q}_{f\beta}\right]_{h_1}, \tag{19}$$

where $\bar{Q} = \sum_{\vec{x}} \bar{q}(\vec{x})$ is the quark wall source. Projection operators for spin-singlet and spin-triplet states are given by

$$P^{S=0}_{\alpha\beta} \equiv \frac{1 - \vec{\sigma}_1 \cdot \vec{\sigma}_2}{4} \quad \text{and} \quad P^{S=1}_{\alpha\beta} \equiv \frac{3 + \vec{\sigma}_1 \cdot \vec{\sigma}_2}{4}. \tag{20}$$

Quark propagators are calculated for the wall source at t_0 with the Dirichlet boundary condition in the temporal direction at $t = 16 + t_0$. The wall source is placed at 32 different values of t_0 on each gauge configuration, in order to increase the statistics, in addition to the average over forward and backward propagations in time. The A_1^+ projection of the cubic group is taken for the sink operator to obtain the relative S-wave in the BB wave function.[2] Numerical computations have been carried out using the KEK supercomputer system, Blue Gene/L, and the kaon and jpsi clusters at Fermilab. The hadron masses obtained in our calculation are given in Table 2. The thresholds of two-baryons with strangeness $S = -2$ for each set of gauge configurations are plotted in Fig. 1.

5. Numerical results

We now present our results of coupled-channel BB potentials in the strangeness $S = -2$ sector.

5.1. Time dependence

We first show how the time-dependent method extended to the coupled-channel system works in our calculation. For this purpose, we investigate the time dependences of the diagonal potentials. Figure 2 shows $V^{\Sigma\Sigma}{}_{\Sigma\Sigma}$ in the ${}^1S_0$ ($I = 2$) channel (5th line in Table 1) and $V^{N\Xi}{}_{N\Xi}$ in the ${}^3S_1$ ($I = 0$) channel (2nd line in Table 1) at three values of $t - t_0$ ($= 8, 9, 10$) with Set 3, which has the lightest pion mass in our calculation. Within statistical errors, no significant $t - t_0$ dependence is observed for these

[2] In this paper, relative D-waves in spin-triplet channels are not explicitly considered, but their effect is included implicitly in the effective central potentials for spin-triplet channels.

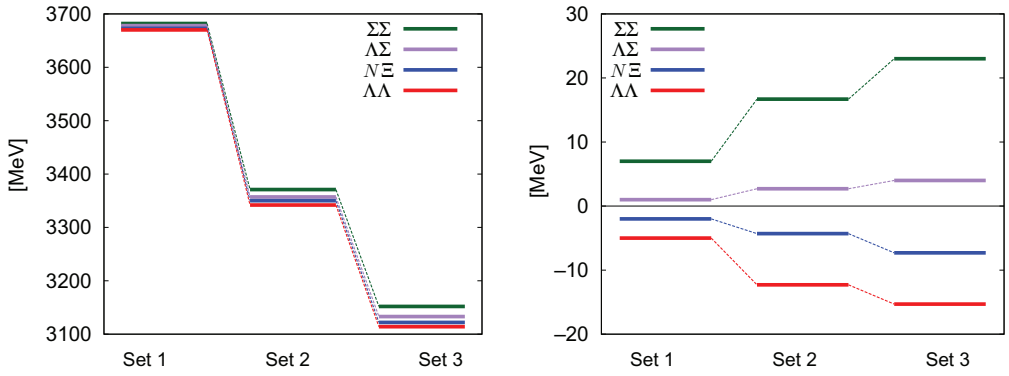

Fig. 1. Thresholds of two-baryons with strangeness $S = -2$ for each gauge ensemble. (Left) The sum of the masses for each channel in units of MeV. (Right) The sum of the two-baryon masses in each channel minus the average of three channels, $(m_N + 2m_\Lambda + m_\Xi + 2m_\Sigma)/3$.

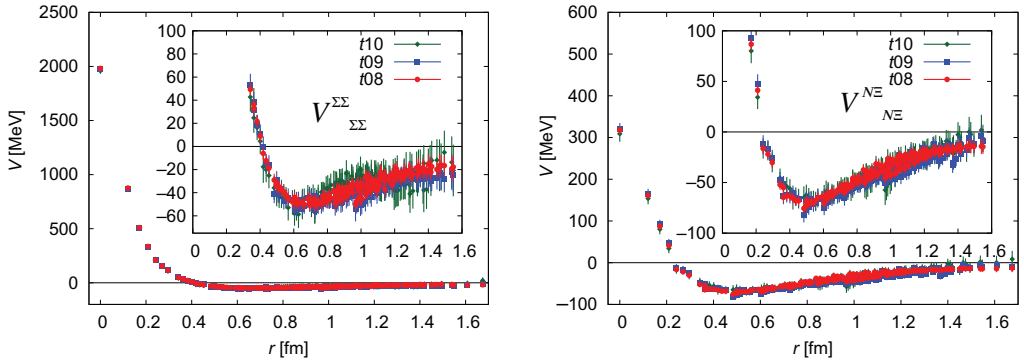

Fig. 2. $\Sigma\Sigma$ potential in the $^1S_0$ ($I = 2$) channel (left) and $N\Xi$ potential in the $^3S_1$ ($I = 0$) channel (right) as a function of r at $t - t_0 = 8$ (red), 9 (blue), and 10 (green) calculated with Set 3.

single-channel potentials with Set 3, showing that $t - t_0 = 8$ is large enough to suppress inelastic contributions and that higher-order contributions in the derivative expansion are negligible.

In Fig. 3, two diagonal potentials in the $^1S_0$ ($I = 1$) channel (3rd line in Table 1) calculated with Set 1 are shown at $t - t_0 = 8$–10. Again, no significant $t - t_0$ dependence is observed at this quark mass and this is true at other quark masses. Similarly, three diagonal potentials in the $^3S_1$ ($I = 1$) channel (4th line in Table 1) and those in the $^1S_0$ ($I = 0$) channel (1st line in Table 1) show no significant $t - t_0$ dependence at all quark masses, as seen in Fig. 4 for Set 2.

Since no significant $t - t_0$ dependences are observed for all diagonal potentials at $t - t_0 = 8, 9, 10$, we hereafter consider the results at $t - t_0 = 8$, where statistical errors are smallest.

5.2. *Hermiticity*

Hermiticity of the potential matrix is a sufficient condition for the probability conservation, though it is not a necessary condition. In this subsection, we investigate the hermiticity of the potential matrix, $V^a{}_b = V^b{}_a$, since it is not automatically guaranteed in the definition of the coupled-channel potential matrix in Eq. (5). As in the case of the diagonal parts, we confirm that the off-diagonal parts of the potential matrix show no significant $t - t_0$ dependence, so we take the results at $t - t_0 = 8$ in our analysis.

We introduce a hermiticity measure $\delta V_{a-b} \equiv 2(V^a{}_b - V^b{}_a)/(V^a{}_b + V^b{}_a)$ to see the relative magnitude of the hermiticiy violation of the potential matrix. Figure 5 presents $\delta V_{N\Xi-\Lambda\Sigma}$ in the $^1S_0$

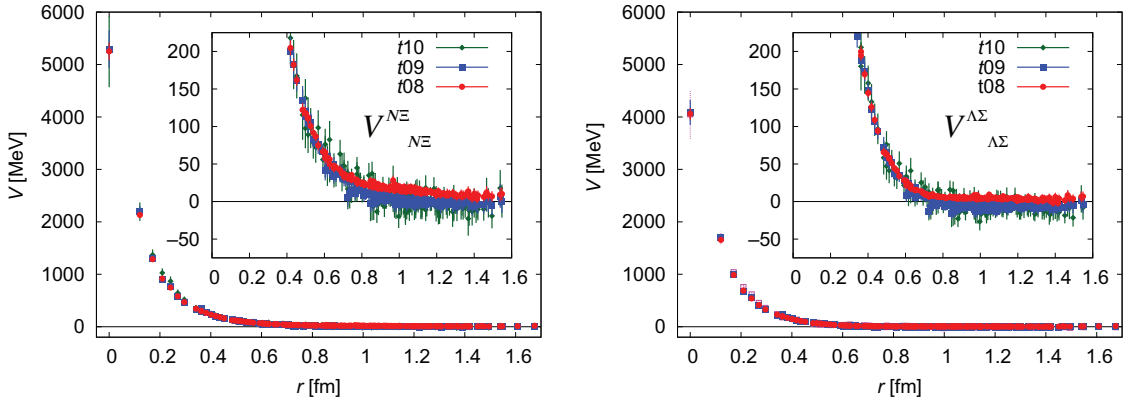

Fig. 3. Diagonal parts of the potential matrix in the ${}^1S_0$ ($I = 1$) channel, $V^{N\Xi}{}_{N\Xi}$ (left) and $V^{\Lambda\Sigma}{}_{\Lambda\Sigma}$ (right), at $t - t_0 = 8$ (red), 9 (blue), and 10 (green) calculated with Set 1.

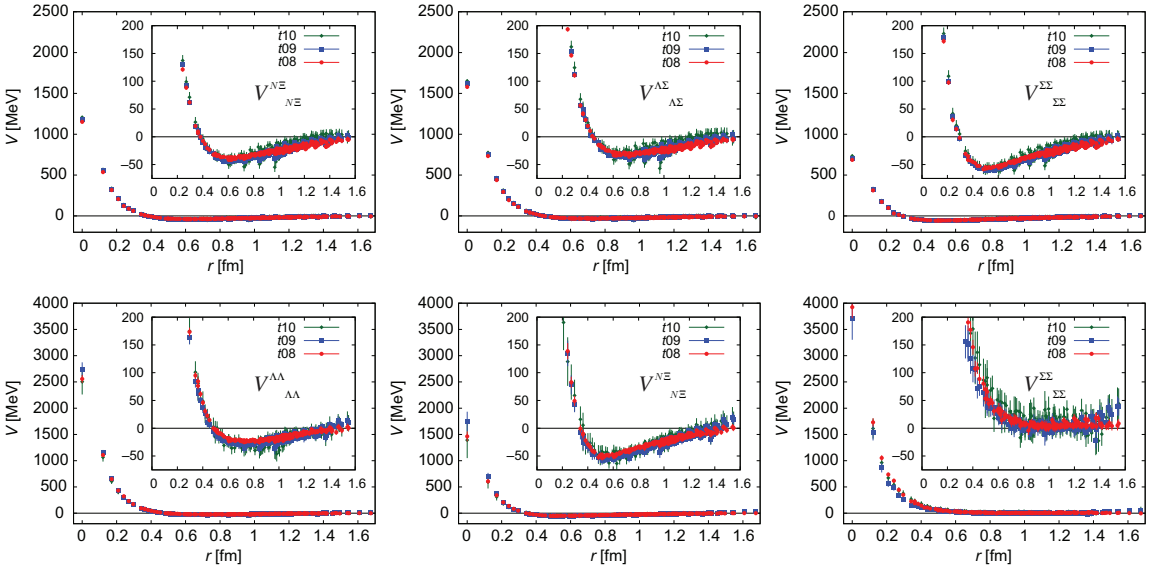

Fig. 4. (Upper) Diagonal parts of the potential matrix in the ${}^3S_1$ ($I = 1$) channel, $V^{N\Xi}{}_{N\Xi}$ (left), $V^{\Lambda\Sigma}{}_{\Lambda\Sigma}$ (center), and $V^{\Sigma\Sigma}{}_{\Sigma\Sigma}$ (right), at $t - t_0 = 8$ (red), 9 (blue), and 10 (green) calculated with Set 2. (Lower) Same as above but in the ${}^1S_0$ ($I = 0$) channel, $V^{\Lambda\Lambda}{}_{\Lambda\Lambda}$ (left), $V^{N\Xi}{}_{N\Xi}$ (center), and $V^{\Sigma\Sigma}{}_{\Sigma\Sigma}$ (right).

($I = 1$) channel with Set 1 (red), Set 2 (blue), and Set 3 (green). It satisfies the hermiticity well within the statistical errors.

Figure 6 shows δV_{a-b} for $a, b = N\Xi, \Lambda\Sigma, \Sigma\Sigma$ in the ${}^3S_1$ ($I = 1$) channel. Some violations of hermiticity can be seen in $\delta V_{N\Xi-\Lambda\Sigma}$ and $\delta V_{\Lambda\Sigma-\Sigma\Sigma}$ in the $r < 0.5$ fm region. Those for $a, b = \Lambda\Lambda, N\Xi, \Sigma\Sigma$ in ${}^1S_0$ ($I = 0$) are given in Fig. 7. Hermiticity is more or less satisfied within the statistical errors. It is a problem for future work to check whether the possible hermiticity breaking for small r in Fig. 6 and large r in Fig. 7 disappears or not by removing our assumption on the wave-function renormalization factor introduced after Eq. (1).

5.3. Potential matrices and their quark mass dependence

We here discuss the properties of potentials in three cases, single channel, two channels, and three channels, separately.

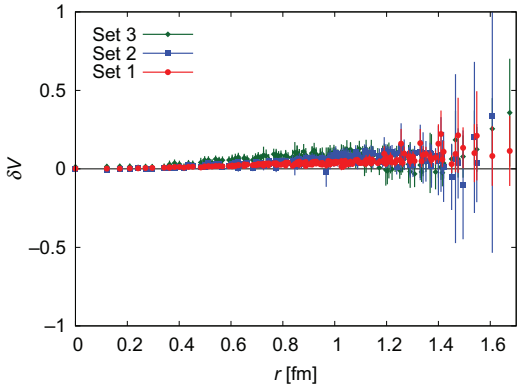

Fig. 5. Hermiticity measure for the off-diagonal elements of the potential matrix, $\delta V_{N\Xi-\Lambda\Sigma}$, in the ${}^1S_0$ ($I = 1$) channel on Set 1 (red), Set 2 (blue), and Set 3 (green).

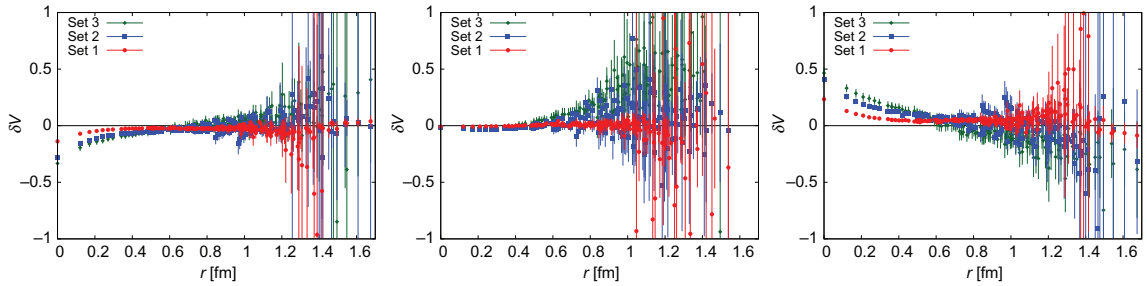

Fig. 6. Violation of hermiticity in the channel ${}^3S_1$ ($I = 1$): (left) $\delta V_{N\Xi-\Lambda\Sigma}$, (center) $\delta V_{N\Xi-\Sigma\Sigma}$, (right) $\delta V_{\Lambda\Sigma-\Sigma\Sigma}$ on Set 1 (red), Set 2 (blue), and Set 3 (green).

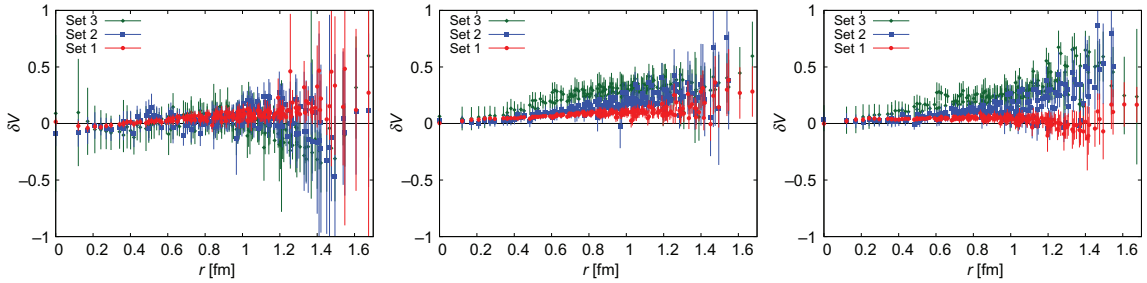

Fig. 7. Violation of hermiticity in the channel ${}^1S_0$ ($I = 0$): (left) $\delta V_{\Lambda\Lambda-N\Xi}$, (center) $\delta V_{\Lambda\Lambda-\Sigma\Sigma}$, (right) $\delta V_{N\Xi-\Sigma\Sigma}$ on Set 1 (red), Set 2 (blue), and Set 3 (green).

5.3.1. Single channel

Figure 8 shows the quark mass dependences of the $\Sigma\Sigma$ potential in the ${}^1S_0$ ($I = 2$) channel (left) and the $N\Xi$ potential in the ${}^3S_1$ ($I = 0$) channel (right). We first notice non-smooth behaviors as a function of r at large r for both cases, which indicates that the spatial volume is not sufficiently large. In addition, the non-smooth behavior at short distance observed in the $N\Xi$ ${}^3S_1$ ($I = 0$) channel may be caused by the finite-lattice-spacing effect. With these systematics, we discuss only the qualitative features of the potentials in this report, and leave quantitative analysis such as the extraction of scattering phase shifts for future studies with larger and finer lattices.

The $\Sigma\Sigma$ potential in the ${}^1S_0$ ($I = 2$) channel (left), which belongs to the 27-plet irreducible representation in the flavor SU(3), has repulsion at short distance and attraction at long distance.

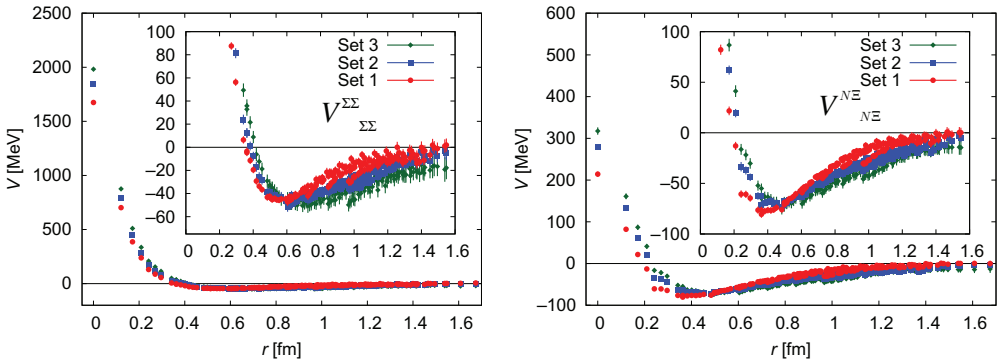

Fig. 8. The $\Sigma\Sigma$ potential in the ${}^1S_0$ ($I = 2$) channel (left) and the $N\Xi$ potential in the ${}^3S_1$ ($I = 0$) channel (right). Results from three gauge ensembles, Set 1 (red), Set 2 (blue), and Set 3 (green), are shown in one figure. The insets show enlargements of the same plot.

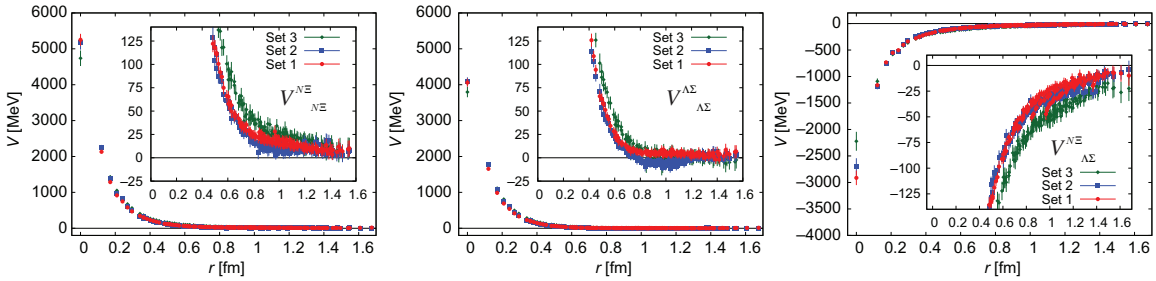

Fig. 9. Diagonal (left and center) and off-diagonal (right) elements of the potential matrix in the ${}^1S_0$ ($I = 1$) channel. Results from three gauge ensembles, Set 1 (red), Set 2 (blue), and Set 3 (green), are shown in one figure. The insets show enlargements of the same plot.

Also, the magnitude of these two components increases as the light (ud) quark mass decreases, as in the case of the NN potential in the ${}^1S_0$ sector belonging to the 27-plet. An increase of attraction at long distance, $r > 0.8$ fm, may be related to the decrease of the mass of the pion exchanged between the two Σ.

Similarly, the $N\Xi$ potential in the ${}^3S_1$ ($I = 0$) channel (right) has both repulsion at short distance and attraction at long distance. The magnitude of these two components is enhanced as the light quark mass decreases. It should be remarked that the repulsion at short distance here is weaker than that of the $\Sigma\Sigma$ potential in the ${}^1S_0$ ($I = 2$) channel. This difference may be related to the fact that the Pauli blocking in the quark level for $N\Xi$ in the ${}^3S_1$ ($I = 0$) channel is weaker than $\Sigma\Sigma$ in the ${}^1S_0$ ($I = 2$) channel.

5.3.2. Two channels

A potential matrix in the ${}^1S_0$ ($I = 1$) channel, which has $N\Xi$ and $\Lambda\Sigma$ components, is given in Fig. 9, which shows that the diagonal elements of the potential matrix in this channel, $V^{N\Xi}{}_{N\Xi}$ and $V^{\Lambda\Sigma}{}_{\Lambda\Sigma}$, are both strongly repulsive and the off-diagonal element, $V^{N\Xi}{}_{\Lambda\Sigma}$, is comparable to or even larger than the diagonal elements. These features have already been observed in the flavor SU(3) symmetric limit [8].

5.3.3. Three channels

Figure 10 shows a potential matrix in the ${}^3S_1$ ($I = 1$) channel, which has $N\Xi$, $\Lambda\Sigma$, and $\Sigma\Sigma$ components. All diagonal elements of the potential matrix, $V^{N\Xi}{}_{N\Xi}$ (left upper), $V^{\Lambda\Sigma}{}_{\Lambda\Sigma}$ (left

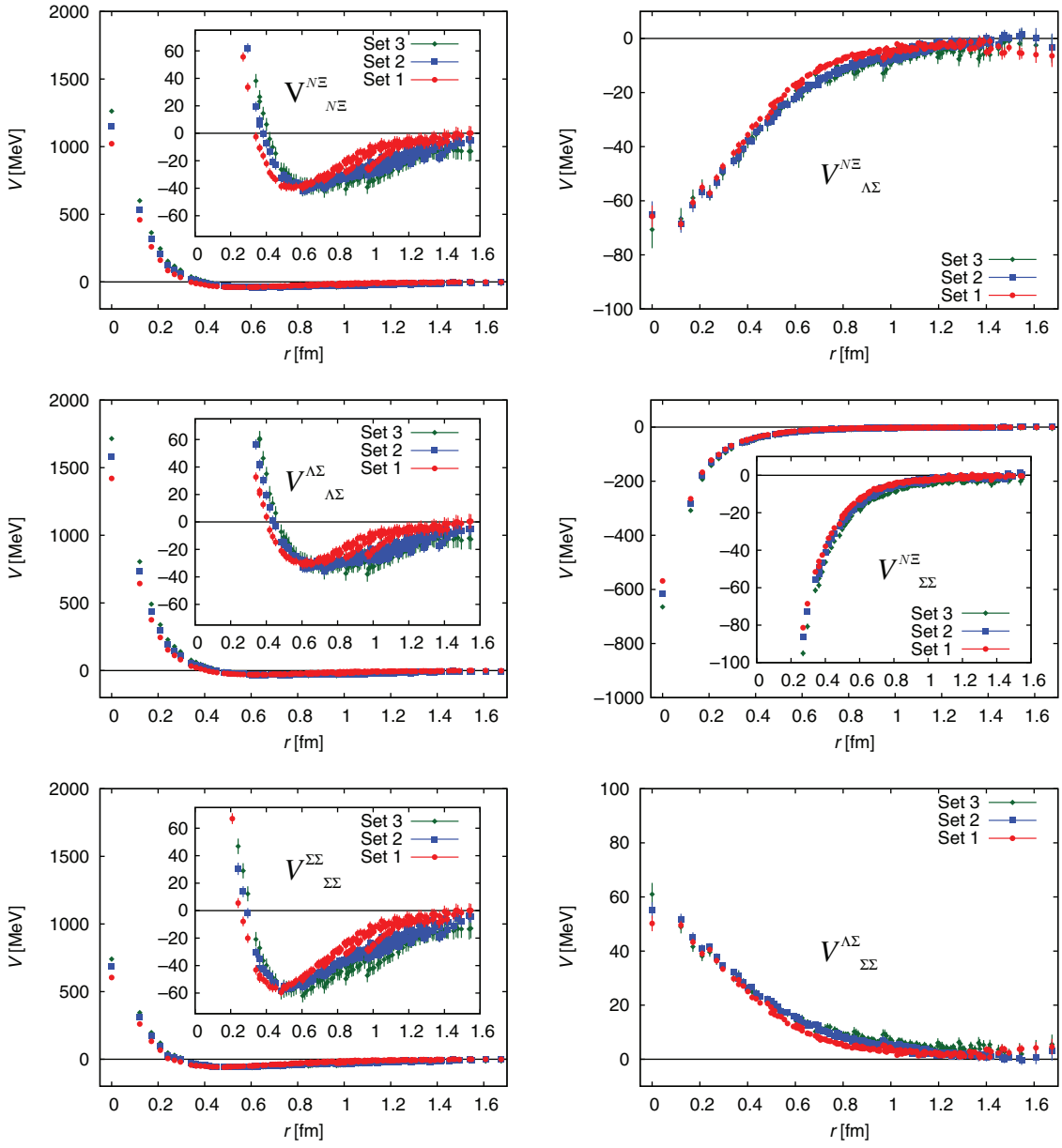

Fig. 10. Diagonal (left three panels) and off-diagonal (right three panels) elements of the potential matrix in the ${}^3S_1$ ($I = 1$) channel. Results from three gauge ensembles, Set 1 (red), Set 2 (blue), and Set 3 (green), are shown in one figure. The insets show enlargements of the same plot.

middle), and $V^{\Sigma\Sigma}{}_{\Sigma\Sigma}$ (left lower), have an attraction at long distance and a repulsive core at short distance. The largest attraction in this channel appears in $V^{\Sigma\Sigma}{}_{\Sigma\Sigma}$, whose maximum depth is about -60 MeV at around $r \sim 0.6$ fm. All the diagonal potentials show a tendency for the magnitudes of both repulsion at short distance and attraction at long distance to increase as the light quark masses decrease.

For the off-diagonal elements of the potential matrix, $V^{N\Xi}{}_{\Lambda\Sigma}$ and $V^{\Lambda\Sigma}{}_{\Sigma\Sigma}$ are much smaller than $V^{N\Xi}{}_{\Sigma\Sigma}$. These off-diagonal potentials, $V^{N\Xi}{}_{\Lambda\Sigma}$ and $V^{\Lambda\Sigma}{}_{\Sigma\Sigma}$, almost vanish at $r > 1.2$ fm and have a small quark mass dependence, while $V^{N\Xi}{}_{\Sigma\Sigma}$ increases as the light quark masses decrease.

Figure 11 shows the potential matrix in the ${}^1S_0$ ($I = 0$) channel, where the H dibaryon state may appear. This potential matrix is also important for the study of double-Λ hypernuclei [23–25]. All

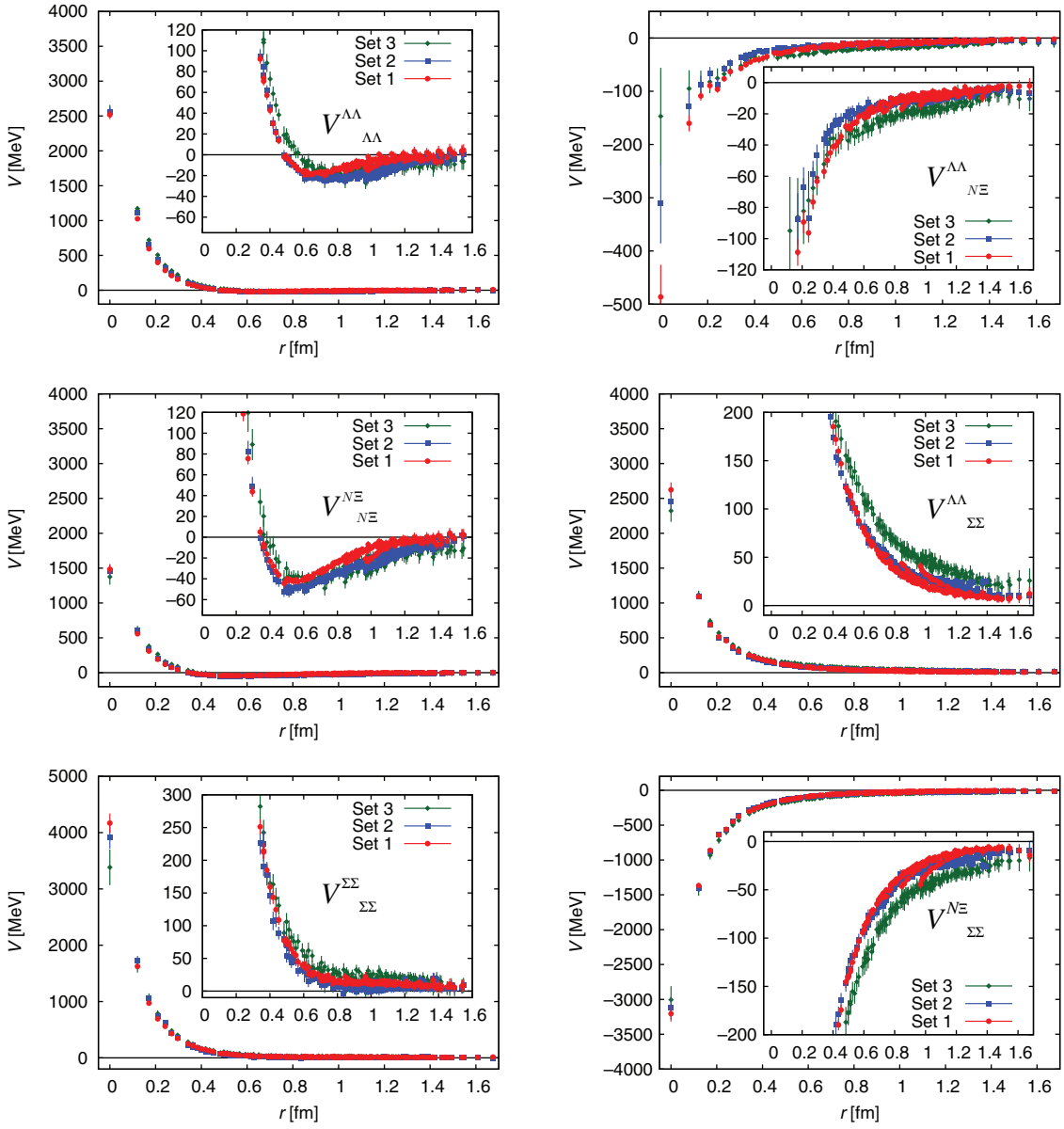

Fig. 11. The potential matrix in the ${}^1S_0$ ($I = 0$) channel, as in Fig. 10.

diagonal elements of the potential matrix have a repulsive core at short distance, whose strength, however, depends strongly on the state. An attractive pocket, on the other hand, appears only in two diagonal elements, $V^{\Lambda\Lambda}{}_{\Lambda\Lambda}$ and $V^{N\Xi}{}_{N\Xi}$, where $V^{N\Xi}{}_{N\Xi}$ has a much deeper attractive pocket than $V^{\Lambda\Lambda}{}_{\Lambda\Lambda}$ does, while $V^{\Sigma\Sigma}{}_{\Sigma\Sigma}$ is totally repulsive in the whole range of r.

The off-diagonal element, $V^{\Lambda\Lambda}{}_{N\Xi}$, is smaller than the other two, so that the decay rate from $N\Xi$ to $\Lambda\Lambda$ may be relatively suppressed. The diagonal elements of the potential matrix generated with the configuration Set 2 are most attractive, while the off-diagonal potentials with the configuration Set 3 are the strongest in magnitude for $r > 0.5$ fm.

We have estimated the volume integral of the diagonal N–Ξ potential with spin and isospin averages. The result shows that there is an overall attraction in all sets. This may have some relevance to the first Ξ hypernucleus recently reported in Ref. [26].

5.4. *Potential matrix in the SU(3) irreducible representation basis*

We here present potential matrices in the SU(3) irreducible representation basis (SU(3) basis for short hereafter) such as 1, 8_s, 8_a, 10, $\overline{10}$, 27, obtained from the particle basis by using Clebsch–Gordan coefficients. This makes it possible for us to compare the results with those in the flavor SU(3) symmetric limit [8].

The transformation from particle basis to SU(3) basis is defined as

$$\left|\begin{matrix}\mathbf{1}\\ \mathbf{8}_s\\ \mathbf{27}\end{matrix}\right\rangle = \begin{pmatrix} -\sqrt{\frac{1}{8}} & \sqrt{\frac{1}{2}} & \sqrt{\frac{3}{8}} \\ -\sqrt{\frac{1}{5}} & \sqrt{\frac{1}{5}} & -\sqrt{\frac{3}{5}} \\ \sqrt{\frac{27}{40}} & \sqrt{\frac{3}{10}} & -\sqrt{\frac{1}{40}} \end{pmatrix} \left|\begin{matrix}\Lambda\Lambda\\ N\Xi\\ \Sigma\Sigma\end{matrix}\right\rangle \tag{21}$$

for the ${}^1S_0(I=0)$ channel, and

$$\left|\begin{matrix}\mathbf{8}_a\\ \mathbf{10}\\ \overline{\mathbf{10}}\end{matrix}\right\rangle = \begin{pmatrix} \sqrt{\frac{1}{3}} & 0 & \sqrt{\frac{2}{3}} \\ -\sqrt{\frac{1}{3}} & \sqrt{\frac{1}{2}} & \sqrt{\frac{1}{6}} \\ -\sqrt{\frac{1}{3}} & -\sqrt{\frac{1}{2}} & \sqrt{\frac{1}{6}} \end{pmatrix} \left|\begin{matrix}N\Xi\\ \Lambda\Sigma\\ \Sigma\Sigma\end{matrix}\right\rangle \tag{22}$$

for the ${}^3S_1(I=1)$ channel.

Figure 12 shows the potential matrix in the SU(3) basis for ${}^3S_1$ $(I=1)$, which is composed of 8_a, 10, and $\overline{10}$. While all the diagonal elements of the potential matrix have a repulsive core, the height of the repulsive core in $V^{8_a}{}_{8_a}$ is much lower than that for the other two and its attractive-pocket depth is the deepest of the three. On the other hand, $V^{10}{}_{10}$ is strongly repulsive and has quite a shallow attractive pocket at all quark masses, though the height of the repulsive core and the range of the attractive pocket increase as the *ud* quark mass decreases. As far as the off-diagonal elements are concerned, they are very small. In particular, $V^{10}{}_{\overline{10}}$ vanishes at all quark masses including Set 3, where the SU(3) breaking by the difference between the *ud* and *s* quark masses is maximal in our calculation. The other two off-diagonal elements, $V^{8_a}{}_{10}$ and $V^{8_a}{}_{\overline{10}}$, have small non-zero values in the short-distance region ($r < 0.6$ fm), which gradually increase as the *ud* quark masses decrease.

Figure 13 shows the potential matrix in the SU(3) basis for ${}^1S_0$ $(I=0)$. As in the case of the SU(3) limit [8], the diagonal element for the flavor singlet state, $V^1{}_1$, is strongly attractive, while $V^{8_s}{}_{8_s}$ is repulsive, at all distances. The absence of a repulsive core in $V^1{}_1$ is consistent with the absence of the quark Pauli blocking effect.[3] The shape of $V^{27}{}_{27}$ is similar to the ${}^1S_0$ nuclear force, which also belongs to the 27-plet.

The quark mass dependences of the diagonal potentials can be clearly seen in the flavor basis. As the light quark mass decreases, the attraction in $V^1{}_1$ gradually increases, while both repulsive core and attraction at long distance in $V^{27}{}_{27}$ are enhanced.

The off-diagonal elements of the potential matrix in the SU(3) basis are presented in the right-hand three panels in Fig. 13, which give effective measures of the flavor SU(3) breaking effects since they are absent in the flavor SU(3) symmetric limit. Figure 13 shows that $V^1{}_{8_s}$ (upper) is small but non-zero, while $V^1{}_{27}$ (middle) and $V^{8_s}{}_{27}$ (lower) are consistent with zero except for very short

[3] Using the $V^1{}_1$ potential with the averaged baryon mass of N, Λ, Σ, Ξ, i.e., $\bar{m} = (2m_N + m_\Lambda + 3m_\Sigma + 2m_\Xi)/8$, we have found one bound state in this fictitious system for all sets of gauge configurations.

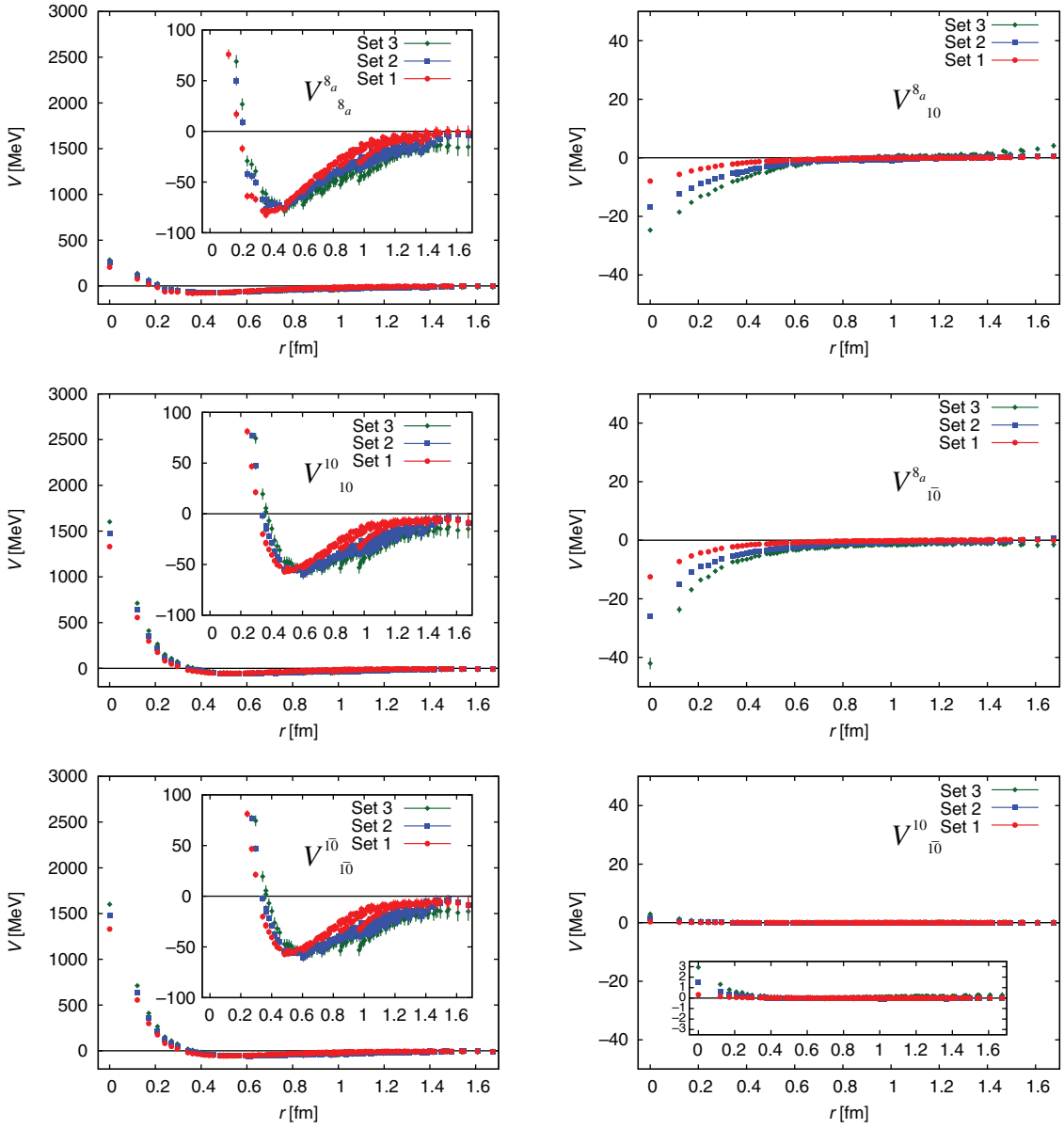

Fig. 12. Potential matrix in the SU(3) basis for ${}^3S_1$ with $S = -2$ and $I = 1$. The left-hand panels are diagonal elements, $V^{8_a}{}_{8_a}$ (upper), $V^{\overline{10}}{}_{\overline{10}}$ (middle), and $V^{10}{}_{10}$ (lower), while the right-hand panels are off-diagonal ones, $V^{8_a}{}_{10}$ (upper), $V^{8_a}{}_{\overline{10}}$ (middle), and $V^{10}{}_{\overline{10}}$ (lower). Red, blue, and green symbols stand for results with Sets 1, 2, and 3, respectively.

distances, $r < 0.2$ fm, where the cutoff effects could be sizable. These results tell us that the flavor SU(3) breaking effects in the off-diagonal parts are much smaller than those in the diagonal part within the quark masses adopted in this paper. The 27-plet state is almost uncoupled even if the ud quark mass is different from the s quark mass.

For ${}^1S_0$ ($I = 1$), the potential matrix in the SU(3) basis is obtained by

$$\left|\begin{matrix} 8_s \\ 27 \end{matrix}\right\rangle = \begin{pmatrix} -\sqrt{\frac{3}{5}} & \sqrt{\frac{2}{5}} \\ \sqrt{\frac{2}{5}} & \sqrt{\frac{3}{5}} \end{pmatrix} \left|\begin{matrix} N\Xi \\ \Lambda\Sigma \end{matrix}\right\rangle. \tag{23}$$

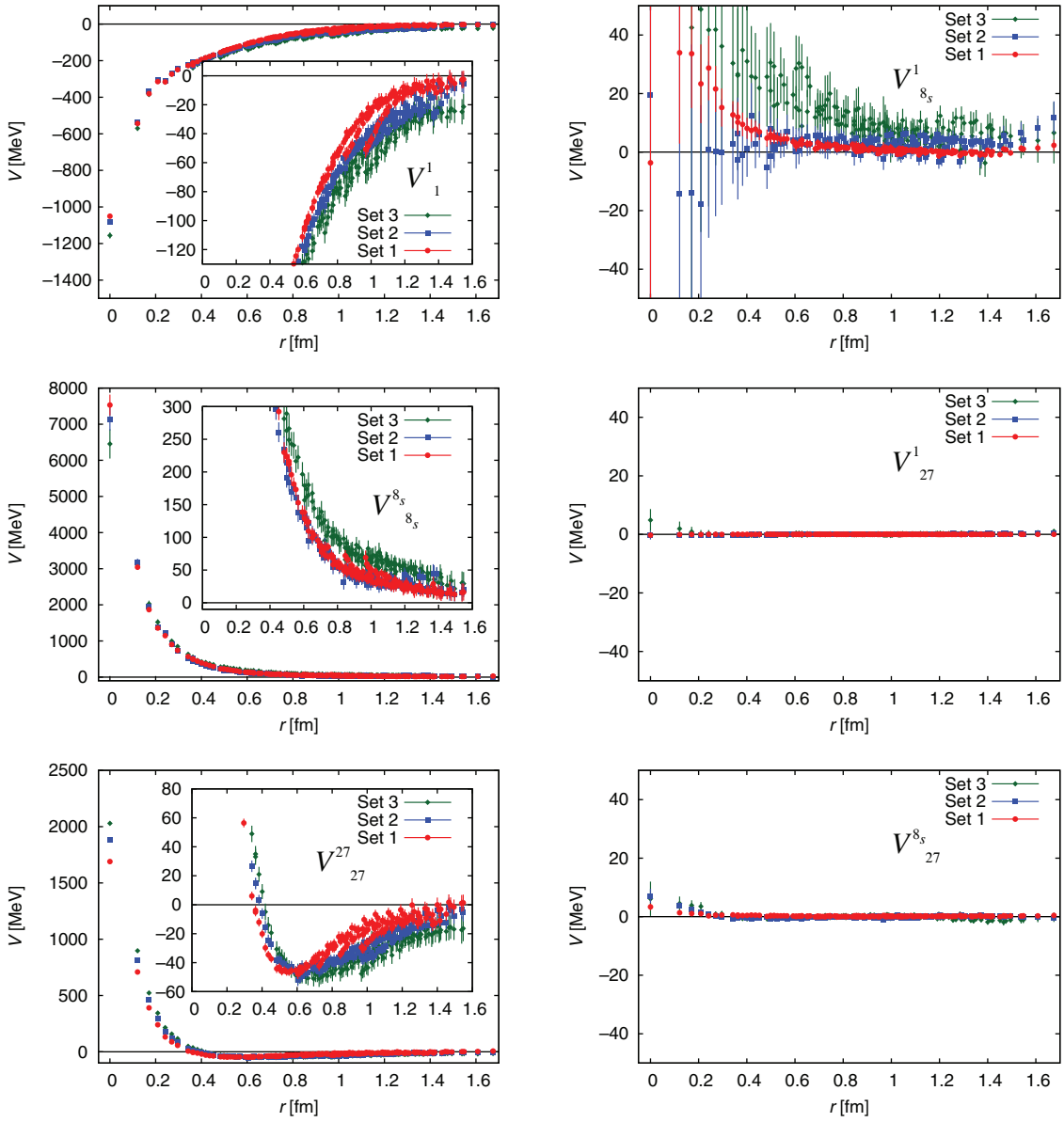

Fig. 13. Potential matrix in the SU(3) basis for ${}^1S_0$ with $S = -2$ and $I = 0$. The left-hand panels are diagonal elements, $V^1{}_1$ (upper), $V^{8_s}{}_{8_s}$ (middle), and $V^{27}{}_{27}$ (lower), while the right-hand panels are off-diagonal ones, $V^1{}_{8_s}$ (upper), $V^1{}_{27}$ (middle), and $V^{8_s}{}_{27}$ (lower). Red, blue, and green symbols stand for results with Sets 1, 2, and 3, respectively.

Figure 14 shows the diagonal and off-diagonal parts of the potential matrix in the SU(3) basis for the ${}^1S_0$ ($I = 1$) channel. We find that the diagonal elements, $V^{8_s}{}_{8_s}$ and $V^{27}{}_{27}$, have similar behaviors to those obtained from ${}^1S_0$ ($I = 0$), and the transition potential between the 8_s-plet and the 27-plet is quite small for all sets.

To see the effects of SU(3) breakings, it is interesting to compare the potentials in the SU(3) basis extracted from two different channels, ${}^1S_0$ ($I = 0$) and ${}^1S_0$ ($I = 1$). In Fig. 15, we show the measure of SU(3) breaking defined as $\Delta V^{(c)} \equiv 2(V^c_{I=0} - V^c_{I=1})/(V^c_{I=0} + V^c_{I=1})$. We find that, for $\Delta V^{(8_s)}$, there are no significant deviations from zero within statistical errors for all sets. Similar behavior to the $\Delta V^{(8_s)}$ case can be seen again for the $\Delta V^{(27)}$ case, except for a singular behavior at $r \simeq 0.4$ fm where the 27-plet potentials themselves almost vanish.

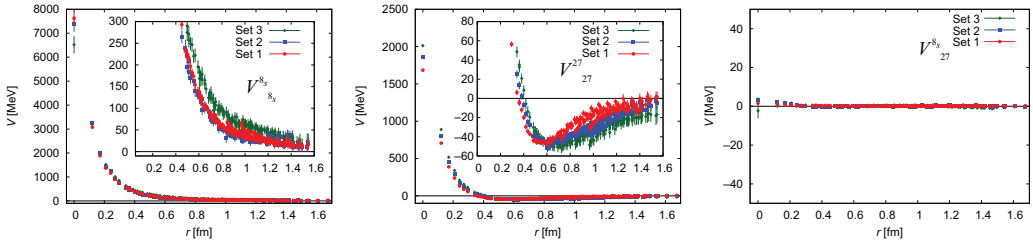

Fig. 14. Diagonal (left and center) and off-diagonal (right) elements of the potential matrix in the SU(3) basis for the ${}^1S_0$ ($I = 1$) channel. Left and center panels are diagonal elements, $V^{8_s}{}_{8_s}$ (left), $V^{27}{}_{27}$ (center), while the right panel is off-diagonal ones, $V^{8_s}{}_{27}$. Red, blue, and green symbols stand for results with Sets 1, 2, and 3, respectively.

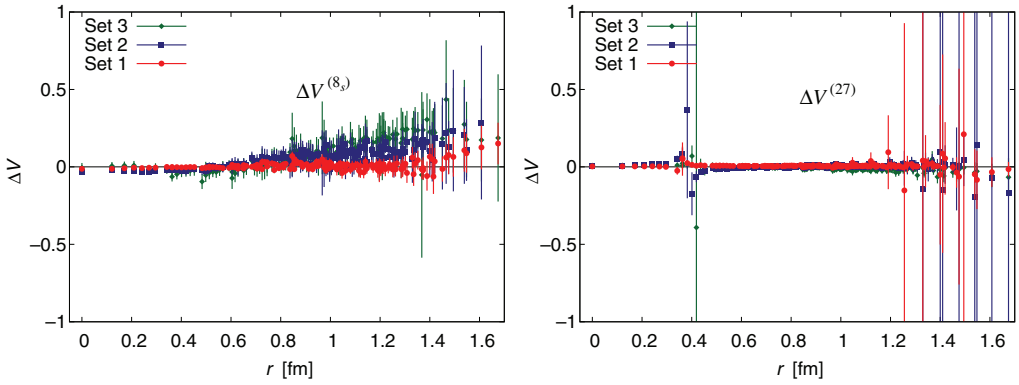

Fig. 15. Measures of SU(3) breaking effects: $\Delta V^{(8_s)}$ (left) and $\Delta V^{(27)}$ (right) as a function of r. Red, blue, and green symbols stand for results with Sets 1, 2, and 3, respectively.

6. Summary and conclusions

In this paper, we have investigated the $S = -2$ BB potentials from $2 + 1$-flavor lattice QCD by using the HAL QCD method extended to coupled-channel systems in Ref. [9]. Combining the coupled-channel formalism with the time-dependent Schrödinger equation [18], we could extract *potential matrices* for the first time without ground-state saturation and without diagonalization of the source operators.

By considering two-baryon systems with $S = -2$, $\Lambda\Lambda$, $N\Xi$, $\Sigma\Sigma$, and $\Lambda\Sigma$, which are mutually coupled, we successfully extracted potential matrices. They are approximately hermitician within the statistical errors, which is not guaranteed from the definition. A small violation of hermiticity may be removed at least partly by proper treatment of the renormalization factors, which is left for future studies.

We have discussed the properties of the potential matrices for all $S = -2$ two-baryon systems. We found that all diagonal elements of the potential matrix have a repulsive core, while their heights largely depend on their flavor structure. Our previous works show that a decreasing ud quark mass leads to an enhancement in the short-range repulsion and the long-range attraction. Although such quark mass dependence was clearly seen in the single-channel case, it becomes less pronounced in the two- and three-channel cases.

The potentials in the SU(3) basis have also been investigated, where we could see clear quark mass dependence. We found a strongly attractive potential for $V^1{}_1$, whose strength increases as the quark mass decreases. The off-diagonal potentials in the SU(3) basis are a proper measure of SU(3)

breaking. In the ${}^3S_1(I = 1)$ channel, except for $V^{\overline{10}}{}_{10}$, only a small transition potential between irreducible representations could be seen at short distances. In the ${}^1S_0(I = 0)$ channel, we found a clear mixture of the flavor singlet state and the octet state. The other off-diagonal potentials have only a small magnitude at short distances. Note, however, that the SU(3) breaking introduced in this paper ($m_\pi/m_K = 0.96, 0.90, 0.86$) is still small compared to the realistic magnitude of the breaking ($m_\pi/m_K = 0.27$). Nevertheless, the present paper provides a first theoretical and numerical step toward a realistic BB potential matrix at physical quark masses.

Acknowledgements

We greatly appreciate the USQCD for their offer of computer resources to overcome the electricity crisis due to the catastrophic earthquake in the east of Japan on 11 March 2011. We are grateful to the authors and maintainers of CPS++ [27], whose modified version is used for our simulations. We also thank the CP-PACS/JLQCD Collaborations and ILDG/JLDG [19,20] for providing gauge configurations. This work is supported in part by the Strategic Program for Innovative Research (SPIRE) Field 5, the Large Scale Simulation Program of the High Energy Accelerator Research Organization (KEK) (Nos. H23:11-14, H23-24:12-11, H24-25:12/13-19, H25-26:13/14-22, H26-27:14/15-21), the Grant-in-Aid of the Ministry of Education, Science and Technology, Sports and Culture (Nos. 19540261, 20340047, 22540268, 24740144, 24740146, 25287046, 25800170, 26400281, 15K17667), and the Grant-in-Aid for Scientific Research on Innovative Areas (Nos. 20105001, 20105003). T.H. was partially supported by the RIKEN iTHES Project.

Funding

Open Access funding: SCOAP[3].

References

[1] C. B. Dover and A. Gal, Annals Phys. **146**, 309 (1983).
[2] B. F. Gibson and E. V. Hungerford, Phys. Rept. **257**, 349 (1995).
[3] E. Hiyama and T. Yamada, Prog. Part. Nucl. Phys. **63**, 339 (2009).
[4] R. L. Jaffe, Phys. Rev. Lett. **38**, 195 (1977); **38**, 617 (1977) [erratum].
[5] T. Sakai, K. Shimizu, and K. Yazaki, Prog. Theor. Phys. Suppl. **137**, 121 (2000) [arXiv:nucl-th/9912063] [Search INSPIRE].
[6] T. Takatsuka, S. Nishizaki, Y. Yamamoto, and R. Tamagaki, Prog. Theor. Phys. **115**, 355 (2006) [arXiv:nucl-th/0601043] [Search INSPIRE].
[7] S. Aoki et al. [HAL QCD Collaboration], Prog. Theor. Exp. Phys. **2012**, 01A105 (2012) [arXiv:1206.5088 [hep-lat]] [Search INSPIRE].
[8] T. Inoue et al. [HAL QCD Collaboration], Nucl. Phys. A **881**, 28 (2012) [arXiv:1112.5926 [hep-lat]] [Search INSPIRE].
[9] S. Aoki et al. [HAL QCD Collaboration], Proc. Jpn. Acad. B **87**, 509 (2011) [arXiv:1106.2281 [hep-lat]] [Search INSPIRE].
[10] S. Aoki, B. Charron, T. Doi, T. Hatsuda, T. Inoue, and N. Ishii, Phys. Rev. D **87**, 034512 (2013) [arXiv:1212.4896 [hep-lat]] [Search INSPIRE].
[11] S. Muroya, A. Nakamura, and J. Nagata, Nucl. Phys. Proc. Suppl. **129**, 239 (2004).
[12] S. R. Beane et al. [NPLQCD Collaboration], Nucl. Phys. A **794**, 62 (2007) [arXiv:hep-lat/0612026] [Search INSPIRE].
[13] S. R. Beane et al., Phys. Rev. Lett. **109**, 172001 (2012) [arXiv:1204.3606 [hep-lat]] [Search INSPIRE].
[14] H. Nemura, N. Ishii, S. Aoki, and T. Hatsuda, Phys. Lett. B **673**, 136 (2009).
[15] H. Nemura, N. Ishii, S. Aoki, and T. Hatsuda, [PACS-CS Collaboration], PoS **LATTICE2008**, 156 (2008).
[16] H. Nemura, [HAL QCD Collaboration and PACS-CS Collaboration], PoS **LATTICE2009**, 152 (2009).
[17] K. Murano, N. Ishii, S. Aoki, and T. Hatsuda, Prog. Theor. Phys. **125**, 1225 (2011) [arXiv:1103.0619 [hep-lat]] [Search INSPIRE].
[18] N. Ishii et al. [HAL QCD Collaboration], Phys. Lett. B **712**, 437 (2012) [arXiv:1203.3642 [hep-lat]] [Search INSPIRE].

[19] International Lattice Data Grid (ILDG), (Available at: http://plone.jldg.org/).
[20] Japan Lattice Data Grid (JLDG), (Available at: http://www.jldg.org/).
[21] CP-PACS/JLQCD Collaborations, (Available at: http://www.jldg.org/ildg-data/CPPACS+JLQCDconfig.html).
[22] T. Ishikawa et al. [CP-PACS/JLQCD Collaboration], Phys. Rev. D **78**, 011502(R) (2008).
[23] E. Hiyama, M. Kamimura, T. Motoba, T. Yamada, and Y. Yamamoto, Phys. Rev. C **66**, 024007 (2002) [arXiv:nucl-th/0204059] [Search INSPIRE].
[24] H. Nemura, Y. Akaishi, and K. S. Myint, Phys. Rev. C **67**, 051001 (2003) [arXiv:nucl-th/0211082] [Search INSPIRE].
[25] H. Nemura, S. Shinmura, Y. Akaishi, and K. S. Myint, Phys. Rev. Lett. **94**, 202502 (2005) [arXiv:nucl-th/0407033] [Search INSPIRE].
[26] K. Nakazawa et al., Prog. Theor. Exp. Phys. **2015**, 033D02 (2015).
[27] Columbia Physics System (CPS), (Available at: http://qcdoc.phys.columbia.edu/cps.html).